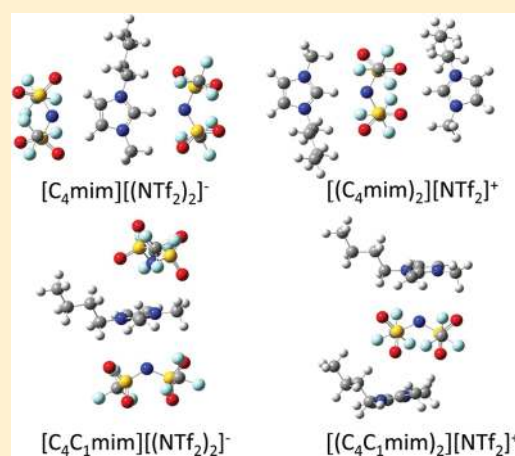


Evaluation of Cation–Anion Interaction Strength in Ionic Liquids

Ana M. Fernandes,^{*,†} Marisa A. A. Rocha,[‡] Mara G. Freire,[§] Isabel M. Marrucho,^{||} João A. P. Coutinho,[§] and Luís M. N. B. F. Santos[‡][†]QOPNA and [§]CICECO, Departamento de Química, Universidade de Aveiro, 3810-193 Aveiro, Portugal[‡]CIQ, Departamento de Química e Bioquímica, Faculdade de Ciências, Universidade do Porto, R. Campo Alegre 687, P-4169-007 Porto, Portugal^{||}Instituto de Tecnologia Química e Biológica, ITQB2, Universidade Nova de Lisboa, Avenida República, 2780-157 Oeiras, Portugal, www.itqb.unl.pt

Supporting Information

ABSTRACT: Electrospray ionization mass spectrometry with variable collision induced dissociation of the isolated [(cation)₂anion]⁺ and/or [(anion)₂cation]⁻ ions of imidazolium-, pyridinium-, pyrrolidinium-, and piperidinium-based ionic liquids (ILs) combined with a large set of anions, such as chloride, tetrafluoroborate, hexafluorophosphate, trifluoromethanesulfonate, and bis[(trifluoromethyl)sulfonyl]imide, was used to carry out a systematic and comprehensive study on the ionic liquids relative interaction energies. The results are interpreted in terms of main influences derived from the structural characteristics of both anion and cation. On the basis of quantum chemical calculations, the effect of the anion upon the dissociation energies of the ionic liquid pair, and isolated [(cation)₂anion]⁺ and/or [(anion)₂cation]⁻ aggregates, were estimated and are in good agreement with the experimental data. Both experimental and computational results indicate an energetic differentiation between the cation and the anion to the ionic pair. Moreover, it was found that the quantum chemical calculations can describe the trend obtained for the electrostatic cation–anion attraction potential. The impact of the cation–anion interaction strengths in the surface tension of ionic liquids is further discussed. The surface tensions dependence on the cation alkyl chain length, and on the anion nature, follows an analogous pattern to that of the relative cation–anion interaction energies determined by mass spectrometry.



INTRODUCTION

The variety of applications of ionic liquids (ILs),^{1–3} virtually covering all areas of chemistry, has contributed to an expanding research on the measurements and simulations of their physical properties, spectroscopic studies, and ab initio calculations. The wide array of combinations between cations, namely, imidazolium-, pyridinium-, pyrrolidinium-, piperidinium-, ammonium-, sulfonium-, and phosphonium-based, and inorganic and organic anions, such as halogens, borates, phosphates, acetates, sulfonates, sulfates, and imides, allows the tuning of physicochemical properties of ionic liquids and their design accordingly to specific purposes.

A fundamental issue in the design of novel ionic liquids is the understanding of the nature/strength of cation–anion interactions and intermolecular forces in the bulk ionic fluid due to their intrinsic relation with most of their physicochemical properties, such as melting temperature, density, viscosity, surface tension, and vapor pressure. In addition, the knowledge of the cation–anion interaction strengths provides valuable information, not only on the characterization of pure ionic liquids properties,

but also on the behavior of systems containing ionic liquids, and how ionic liquids interact with other solvents.

Ab initio and density functional theory based (DFT-based) quantum chemical methods have been used in the past decade to study the energetics of ionic liquids, and the performance of a range of DFT functionals has been recently analyzed to identify the most adequate in providing ionic liquids binding energies.⁴ Several publications dealing with the relationship of cation (ring type and/or alkyl chain length) and anion structures of ILs with their physicochemical properties, namely, melting point, density, viscosity, surface tension, conductivity, self-diffusion coefficient, and heat of vaporization, among others, are already available.^{5–14}

Mass spectrometry, namely, electrospray tandem mass spectrometry (ESI-MS-MS), with energy variable collision induced dissociation, is typically used in the determination of relative binding energies of gas-phase ions in a semiquantitative way. The

Received: February 1, 2011

Revised: March 3, 2011

Published: March 22, 2011

production of gas-phase ions from ionic solutions in the electro-spray ionization process involves two main steps: (a) production of charged droplets at the capillary tip and (b) shrinkage of charged droplets due to solvent evaporation, and repeated droplet fission, leading to gas-phase ions that can be analyzed in the mass spectrometer. The concept of tandem mass spectrometry is the mass selection of a particular ion (precursor ion) produced in the ion source, which is afterward collided with a rare gas, for instance argon, in order to increase its internal energy. The resulting fragments are evaluated in a second analyzer (or in the same analyzer, depending on the type of instrument used). The laboratory frame collision energy (E_{lab}) can be easily changed, which will also produce a variation in the collision energy fraction that is actually converted to the ions' internal energy. The variable collision energies in the ESI-MS-MS spectra will be evident from the relative abundances of precursor and fragment ions, while the energy value corresponding to a relative abundance of the precursor ion of 50% ($E_{1/2}$) can be used as a measure of the relative dissociation energy. This method^{15,16} has already proved to be an adequate strategy in the study of the relative binding energies/stabilities of flavonoid/transition metal complexes,¹⁷ pyridyl ligand/metal complexes,¹⁸ noncovalent complexes,^{19,20} nitrogen bases to metalloporphyrin cations,²¹ quadruplex DNA structures,²² alkali metal complexes of polyether ionophore antibiotics,²³ ionic liquid aggregates,²⁴ and hydrogen-bonding interactions between polyethers and protonated amines or peptides.²⁵

This work presents energy variable collision induced dissociation measurements for the ionic liquid isolated ions, [(cation)₂anion]⁺ and [(anion)₂cation]⁻, aiming at providing fundamental insights into the relative cation–anion interaction strengths. As a result, the differences in binding energies were evaluated by making use of the structural features of the ionic species, such as the cation core and ring size, aromaticity, alkyl chain length, anion nature and size, and ion charge densities. Quantum chemical calculations were used to calculate the dissociation energies of the ionic liquid ion pairs and isolated [(cation)₂anion]⁺ and [(anion)₂cation]⁻ aggregates. In addition, the interaction strengths obtained in this study were correlated with the ionic liquid surface tensions.

EXPERIMENTAL SECTION

Materials. The cation/anion combinations of the ionic liquids studied in this work, as well as respective abbreviations and molecular structures, are listed in Table 1. ILs were purchased from IoLiTec (Freiburg, Germany) or Solchemar (Lisboa, Portugal). All ionic liquid samples presented mass fraction purities > 99% as confirmed by us by ¹H and ¹³C NMR spectroscopy.

Experimental Procedure. Electrospray ionization tandem mass spectra (ESI-MS-MS) were acquired with a Micromass Q-ToF 2 (Micromass, Manchester, U.K.), operating in the positive (or negative) ion mode, equipped with a Z-spray source. Source and desolvation temperatures were 353 and 373 K, respectively. Ionic liquid solutions in methanol, at concentrations of $\sim 10^{-4}$ mol · dm⁻³, were introduced at a 10 mm³ · min⁻¹ flow rate. The capillary and the cone voltage were 2600 V (or 3000 V) and 30 V, respectively. Nitrogen was used as the nebulization gas and argon as the collision gas.

ESI-MS-MS spectra were acquired by selecting the precursor ion with the quadrupole and performing collisions in the hexapole with argon at variable energies. Each spectrum represents an average of approximately 100 scans, and the values of $E_{\text{lab},1/2}$ were determined as the collision energy at which the relative abundance of the precursor ion is 50%. Triplicate measurements were performed for each selected precursor ion, and standard deviations that varied between 0.3 and 5% were obtained.

COMPUTATIONAL DETAILS

Quantum chemical calculations were performed using density functional theory with the hybrid exchange correlation functional (B3LYP).^{26,27} The geometry optimizations were carried out using the B3LYP/6-31+G(d) level of theory. At the same level of theory, the fundamental vibrational frequency calculations were carried out to ensure the true minima. The total electronic energies for each isolated ionic liquid, and for each [(cation)₂-anion]⁺ and [(anion)₂cation]⁻ aggregate, were corrected with the basis set superposition error (BSSE) using the Boys–Bernardi counterpoise technique.²⁸ All theoretical calculations were performed using the Gaussian 03 software package.²⁹

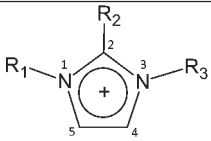
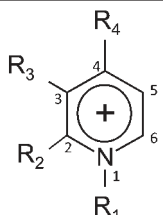
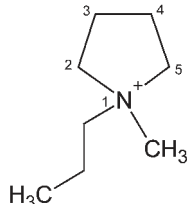
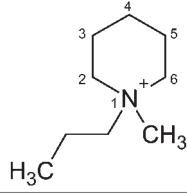
RESULTS AND DISCUSSION

Mass Spectrometry. The ESI mass spectra of all of the studied ionic liquids show, both in the positive and negative ion mode, peaks corresponding to the isolated cation (or anion) and to ionic liquid aggregates. Our experimental strategy for the proposed study involved the selection of the aggregate [(cation)₂anion]⁺ (or [cation(anion)₂]⁻) with the first quadrupole of the mass spectrometer, followed by collisional activation with argon in the hexapole, and further analysis of the fragments with the time-of-flight (TOF) analyzer. All of the ions dissociate by loss of a neutral ionic liquid molecule (Figure 1). To implement energy variable collision induced dissociation, the applied collisional activation voltage (E_{lab}) is increased by small increments, while the relative abundances of the precursor and fragment ions are monitored. The energy required to dissociate 50% of the precursor ion was registered as $E_{\text{lab},1/2}$. In this inelastic collision of the projectile ion with the target neutral, the total available energy for conversion of translational (or kinetic) to internal (or vibrational) energy of the projectile ion is the center of mass energy (E_{cm}), which can be calculated from E_{lab} , and from the masses of the neutral target (m_t) and precursor ion (m_p), by the following,³⁰

$$E_{\text{cm}} = E_{\text{lab}} \left(\frac{m_t}{m_p + m_t} \right) \quad (1)$$

The calculated dissociation energies from the experimental E_{lab} values represent the energy necessary to separate a cation (or anion) from the neutral ionic liquid molecule in the gas phase and, as such, can be considered a good approximation to the cation–anion interaction energy. It should be remarked that besides the Coulombic (electrostatic) interactions, which are considered to be the major source of attraction in ionic liquids,⁹ additional interactions such as van der Waals interactions between alkyl chains, π – π stacking interactions and hydrogen-bonding between polar groups, are also present.

Table 1. Ionic Structures and Respective Abbreviations for the Studied Ionic Liquids

| Imidazolium-based Cations | | | | |
|---|---------------------------|---------------------------|---------------------------|---|
|  | | | | |
| R ₁ : methyl | R ₂ : hydrogen | R ₃ : methyl | | [C ₁ mim] ⁺ |
| R ₁ : ethyl | R ₂ : hydrogen | R ₃ : methyl | | [C ₂ mim] ⁺ |
| R ₁ : propyl | R ₂ : hydrogen | R ₃ : methyl | | [C ₃ mim] ⁺ |
| R ₁ : butyl | R ₂ : hydrogen | R ₃ : methyl | | [C ₄ mim] ⁺ |
| R ₁ : pentyl | R ₂ : hydrogen | R ₃ : methyl | | [C ₅ mim] ⁺ |
| R ₁ : hexyl | R ₂ : hydrogen | R ₃ : methyl | | [C ₆ mim] ⁺ |
| R ₁ : heptyl | R ₂ : hydrogen | R ₃ : methyl | | [C ₇ mim] ⁺ |
| R ₁ : octyl | R ₂ : hydrogen | R ₃ : methyl | | [C ₈ mim] ⁺ |
| R ₁ : decyl | R ₂ : hydrogen | R ₃ : methyl | | [C ₁₀ mim] ⁺ |
| R ₁ : ethyl | R ₂ : hydrogen | R ₃ : ethyl | | [C ₂ C ₂ im] ⁺ |
| R ₁ : butyl | R ₂ : methyl | R ₃ : methyl | | [C ₄ C ₁ mim] ⁺ |
| Pyridinium-based Cations | | | | |
|  | | | | |
| R ₁ : butyl | R ₂ : hydrogen | R ₃ : hydrogen | R ₄ : hydrogen | [C ₄ py] ⁺ |
| R ₁ : hexyl | R ₂ : hydrogen | R ₃ : hydrogen | R ₄ : hydrogen | [C ₆ py] ⁺ |
| R ₁ : octyl | R ₂ : hydrogen | R ₃ : hydrogen | R ₄ : hydrogen | [C ₈ py] ⁺ |
| R ₁ : propyl | R ₂ : hydrogen | R ₃ : methyl | R ₄ : hydrogen | [C ₃ mpy] ⁺ |
| R ₁ : butyl | R ₂ : hydrogen | R ₃ : methyl | R ₄ : hydrogen | [1-C ₄ -3-mpy] ⁺ |
| R ₁ : butyl | R ₂ : hydrogen | R ₃ : hydrogen | R ₄ : methyl | [1-C ₄ -4-mpy] ⁺ |
| Pyrrolidinium-based Cations | | | | |
|  | | | | |
| R ₁ : methyl | | | | |
| R ₁ : propyl | | | | [C ₃ mpyr] ⁺ |
| Piperidinium-based Cations | | | | |
|  | | | | |
| R ₁ : methyl | | | | |
| R ₁ : propyl | | | | [C ₃ mpip] ⁺ |
| Anions | | | | |
| chloride, Cl ⁻ | | | | trifluoromethanesulfonate, [CF ₃ SO ₃] ⁻ , [TfO] ⁻ |
| tetrafluoroborate, [BF ₄] ⁻ | | | | bis[(trifluoromethyl)sulfonyl]imide, |
| hexafluorophosphate, [PF ₆] ⁻ | | | | [N(CF ₃ SO ₂) ₂] ⁻ , [NTf ₂] ⁻ |

The discussion of the experimental results obtained will be organized in terms of the influence of the following structural features of ionic liquids: (a) alkyl chain length in the

imidazolium cation for the ionic liquids [C_nmim][NTf₂] (*n* = 1–10); (b) IL structural and positional isomerism at the cation; (c) IL cation core (imidazolium-, pyridinium-, pyrrolidinium-, and

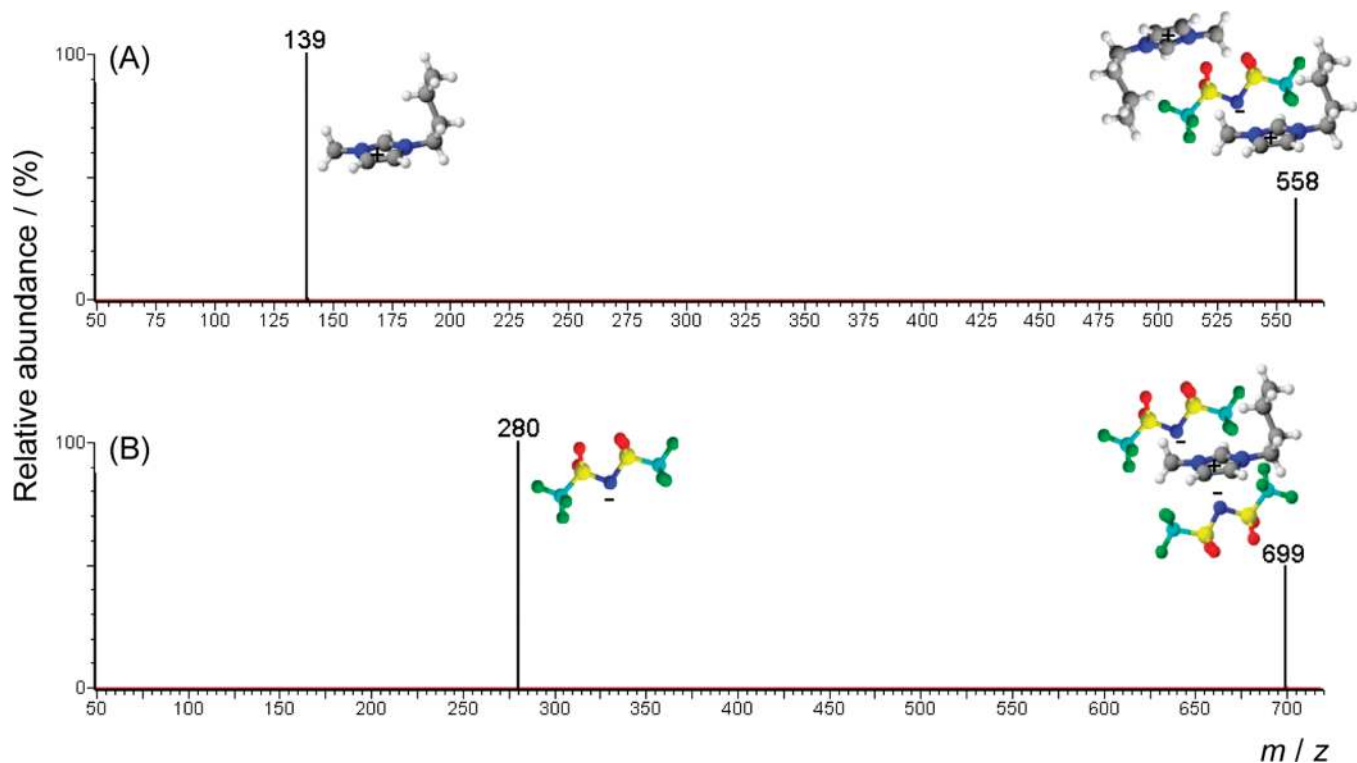


Figure 1. ESI-MS-MS of $[(C_4mim)_2NTf_2]^+$ in the positive ion mode at 7 eV collision energy (A) and $[C_4mim(NTf_2)_2]^-$ in the negative ion mode at 7 eV collision energy (B).

piperidinium-based) with the fixed $[NTf_2]^-$ counterion; (d) anion type for $[C_nmim]$ -based ILs combined with Cl^- , $[BF_4]^-$, $[PF_6]^-$, $[TfO]^-$, and $[NTf_2]^-$.

The calculated dissociation energies, $E_{cm,1/2}$, and the experimental $E_{lab,1/2}$ values for the ions composed of two cations and one anion, or two anions and one cation (only for the imidazolium-based ionic liquids), are listed in Table 2. It should be noted that both energies were determined at a relative abundance of the precursor ion at 50%.

Analysis of the data for the imidazolium-based series of ionic liquids, $[C_nmim][NTf_2]$, reveals different trends for the variation of the interaction energy with the cation alkyl chain length, when considering the dissociation of either $[(cation)_2anion]^+$ or $[cation(anion)_2]^-$. The energy required for the separation of the anion from the neutral molecule within the anionic aggregate is practically independent of the alkyl chain length, whereas in the separation of the cation from the neutral molecule within the cationic aggregate, the energy decreases from $[C_1mim][NTf_2]$ to $[C_5mim][NTf_2]$ toward a constant value for higher values of n in $[C_nmim][NTf_2]$, as depicted in Figure 2. When considering the dissociation energies for the $[(cation)_2anion]^+$ aggregates, the presence of two cations enhances the steric hindrance, which in turns causes an increase in the distance between the ions, and therefore leads to a decrease in the relative ionic interactions. This effect is particularly notorious as the cation alkyl chain length increases from $[C_1mim][NTf_2]$ to $[C_5mim][NTf_2]$. For longer alkyl chains at the imidazolium cation, a further extension of the chain away from the ring, where the interaction with the anion predominantly occurs, does not produce any significant effect. Aiming at complementing this study, the influence of the anion on this trend was further investigated by replacing the

Table 2. $E_{lab,1/2}$ and $E_{cm,1/2}$ Values for the Dissociation of the Ions $[(cation)_2anion]^+$ and $[cation(anion)_2]^-$

| ionic liquid | $[(cation)_2anion]^+$ | | $[cation(anion)_2]^-$ | |
|------------------------|-----------------------|-----------------|-----------------------|-----------------|
| | $E_{lab,1/2}/eV$ | $E_{cm,1/2}/eV$ | $E_{lab,1/2}/eV$ | $E_{cm,1/2}/eV$ |
| $[C_1mim][NTf_2]$ | 9.4 | 0.73 | 6.7 | 0.39 |
| $[C_2mim][NTf_2]$ | 8.3 | 0.61 | 6.7 | 0.38 |
| $[C_3mim][NTf_2]$ | 7.8 | 0.54 | 6.8 | 0.38 |
| $[C_4mim][NTf_2]$ | 7.3 | 0.49 | 6.9 | 0.37 |
| $[C_5mim][NTf_2]$ | 7.2 | 0.46 | 7.1 | 0.38 |
| $[C_6mim][NTf_2]$ | 7.4 | 0.45 | 7.2 | 0.37 |
| $[C_7mim][NTf_2]$ | 7.6 | 0.45 | 7.3 | 0.38 |
| $[C_8mim][NTf_2]$ | 7.6 | 0.43 | 7.5 | 0.38 |
| $[C_{10}mim][NTf_2]$ | 8.5 | 0.44 | 7.7 | 0.37 |
| $[C_2C_2im][NTf_2]$ | 7.5 | 0.53 | 6.6 | 0.37 |
| $[C_4C_1mim][NTf_2]$ | 6.7 | 0.43 | | |
| $[C_3mpyr][NTf_2]$ | 9.0 | 0.62 | | |
| $[C_3mpip][NTf_2]$ | 8.8 | 0.58 | | |
| $[C_4py][NTf_2]$ | 7.4 | 0.50 | | |
| $[C_6py][NTf_2]$ | 7.3 | 0.45 | | |
| $[C_8py][NTf_2]$ | 7.9 | 0.45 | | |
| $[C_3mpy][NTf_2]$ | 7.0 | 0.47 | | |
| $[1-C_4-3-mpy][NTf_2]$ | 6.8 | 0.44 | | |
| $[1-C_4-4-mpy][NTf_2]$ | 7.0 | 0.45 | | |
| $[C_4mim]Cl$ | 8.8 | 0.82 | | |
| $[C_4mim][BF_4]$ | 8.3 | 0.67 | | |
| $[C_4mim][PF_6]$ | 8.9 | 0.63 | | |
| $[C_4mim][TfO]$ | 8.5 | 0.60 | | |

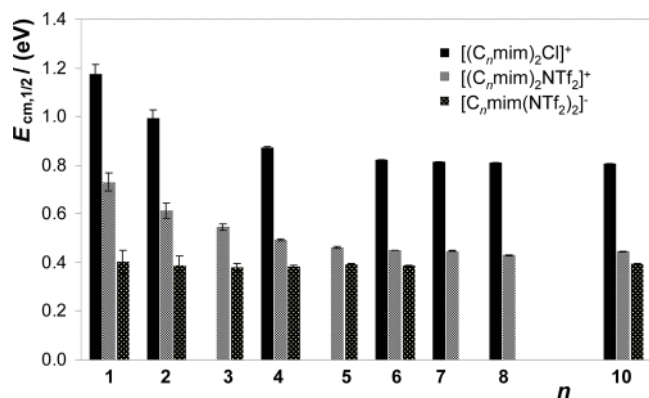


Figure 2. $E_{cm,1/2}$ dependence with the alkyl chain length in $[(C_n\text{mim})_2\text{Cl}]^+$ and $[(C_n\text{mim})_2\text{NTf}_2]^+$ in the positive and negative ion mode.

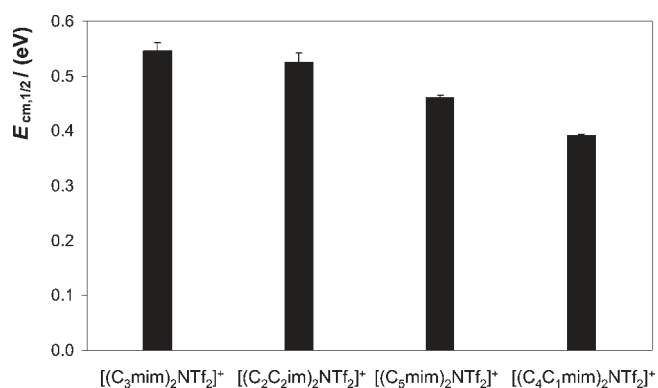


Figure 3. $E_{cm,1/2}$ for isomeric structures of imidazolium-based ILs in the positive ion mode ($[(C_3\text{mim})_2\text{NTf}_2]^+$ compares to $[(C_2C_2\text{im})_2\text{NTf}_2]^+$ while $[(C_5\text{mim})_2\text{NTf}_2]^+$ compares to $[(C_4C_1\text{mim})_2\text{NTf}_2]^+$).

bulky [bis(trifluoromethylsulfonyl)]imide by the chloride anion. The results presented in Figure 2 for chloride-based ILs display the same behavior observed for the $[\text{NTf}_2]$ -based counterparts, showing that the anion type/size is not determinant.

Although cation–anion interactions in ionic liquids are mainly dominated by Coulombic forces, the hydrogen bonding also plays an important role. For imidazolium-based ionic liquids the hydrogen bonding between the cation and the anion is mainly determined by the most acidic hydrogen at the cation in the position C2. This effect is evident when comparing the data shown in Figure 3, where the effect of substituting a hydrogen at the C2 position by a methyl group is displayed. The $[(C_4C_1\text{mim})_2\text{NTf}_2]^+$ is a structural isomer of $[(C_5\text{mim})_2\text{NTf}_2]^+$ and their values of $E_{cm,1/2}$ are displayed in Table 2. Particularly, $[(C_4C_1\text{mim})_2\text{NTf}_2]^+$ has a lower interaction energy compared with its structural isomer, emphasizing the importance of the hydrogen bonding between ions.

The remaining studies for other structural isomers of the imidazolium-based ILs, which do not involve the presence of alkyl groups at the position C2 ($[(C_2C_2\text{im})_2\text{NTf}_2]^+$ and $[(C_3\text{mim})_2\text{NTf}_2]^+$), depicted in Figure 3, do not show significant differences in their relative ionic interaction strengths. Indeed, for both structural isomers the cation–anion interaction strengths are within the associated standard deviations.

The influence of the cation core on the dissociation energies of $[(\text{cation})_2\text{anion}]^+$ aggregates was investigated using pyrrolidinium-,

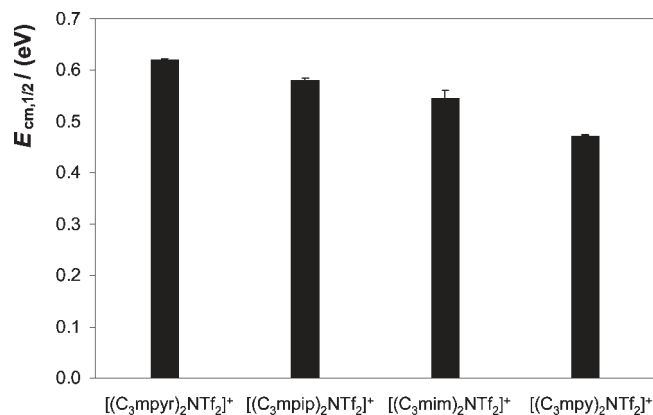


Figure 4. $E_{cm,1/2}$ for pyrrolidinium-, piperidinium-, imidazolium-, and pyridinium-based ionic liquids in the positive ion mode.

piperidinium-, imidazolium-, and pyridinium-based ionic liquids with the [bis(trifluoromethylsulfonyl)imide] fixed anion. The relative cation–anion interaction strength results, in terms of $E_{cm,1/2}$, are displayed in Figure 4. The reduction of the electrostatic strength due to the charge delocalization in aromatic rings, as compared to a localized charge on the nitrogen atom of saturated rings, is reflected on the relative values of interaction energies. Aromatic-based ILs (pyridinium- and imidazolium-based) present lower relative interaction strength values when compared with their saturated counterparts (piperidinium- and pyrrolidinium-based). A similar effect has been reported in the correlation between proton affinity and charge delocalization of ionic liquid anions, whereby a greater degree of delocalization lowers the proton affinity.³¹ The cation size increase from a five- to a six-membered ring, in both aromatic and saturated cores, increases the distance between charges while delocalizing them as well, resulting thus in a decrease in the ionic interaction energy. Curiously, this effect is similar to that observed for the increase of the cation side alkyl chain length.

Aiming at exploring the alkyl chain length influence with a different cation core, and the structural/positional isomerism on the dissociation energies, the pyridinium-based ionic liquids were additionally investigated (Figure 5). The $E_{cm,1/2}$ values obtained for the pyridinium-based ionic liquids show a variation with the alkyl chain length (see results for $[(C_4\text{py})\text{NTf}_2]^+$, $[(C_6\text{py})\text{NTf}_2]^+$, and $[(C_8\text{py})\text{NTf}_2]^+$) similar to that previously discussed for the imidazolium-based ILs. Although the studied pyridinium are alkyl monosubstituted cations, while the imidazolium presented before were alkyl-dissubstituted, this effect seems to be independent of the number of alkyl groups present at the cation.

Regarding the effect of structural isomerism on the ionic interactions, it is visible from Figure 5 that a second alkyl substitution on the aromatic ring with a methyl group decreases the interaction energy (compare $[(1-C_3-3\text{mpy})\text{NTf}_2]^+$ with $[(C_4\text{py})\text{NTf}_2]^+$). This trend can be associated with two cumulative effects: inductive effect of the second substitution with the methyl group that reduces the overall net charge on the cation ring through electron release, and decrease of the charged anion and cation distance due to the presence of an isolated bulkier group. For the positional pair of isomers, $[(1-C_4-4\text{mpy})\text{NTf}_2]^+$ and $[(1-C_4-3\text{mpy})\text{NTf}_2]^+$, a decrease in the relative interaction strength was observed for the meta-substituted IL, $[(1-C_4-3\text{mpy})\text{NTf}_2]^+$. The dialkyl substitutions at positions C1 and C4 in the pyridinium cation (see Table 1) lead to an enhanced

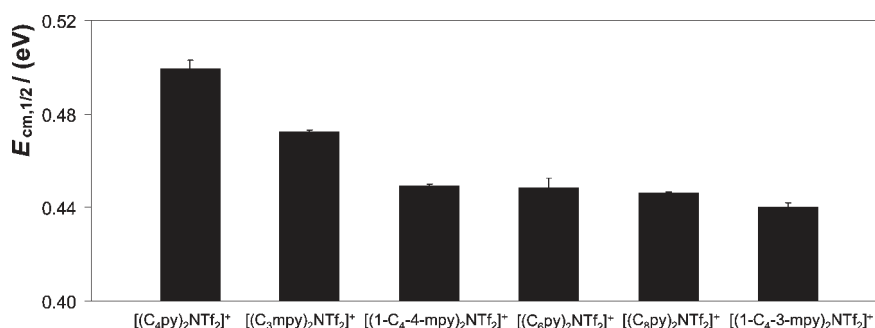


Figure 5. $E_{\text{cm},1/2}$ as a function of the alkyl chain length, and structural and positional isomeric effects, for pyridinium-based ionic liquids in the positive ion mode.

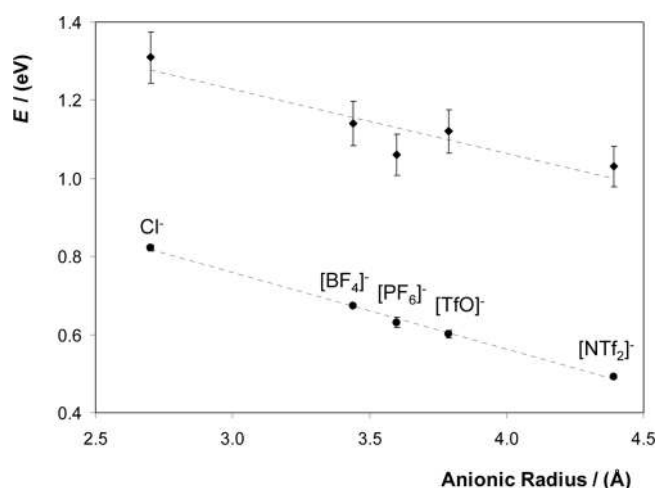


Figure 6. Cation–anion interaction energy as a function of the anionic radius in the $[\text{cation}(\text{anion})_2]^-$ aggregates of the $[\text{C}_4\text{mim}]$ -based ILs combined with the anions Cl^- , $[\text{BF}_4]^-$, $[\text{PF}_6]^-$, $[\text{TfO}]^-$, and $[\text{NTf}_2]^-$: (◆) $E_{\text{diss(BSSE)}}$, dissociation energies calculated at B3LYP/6-31+G(d) level of theory (uncertainty in the order of 5%); (●) $E_{\text{cm},1/2}$, experimental relative interaction energies.

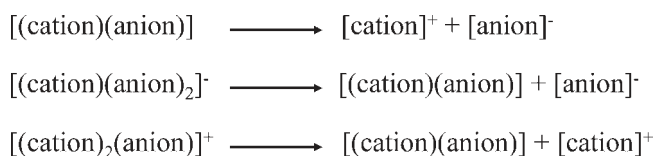
distribution of charge, or to a high charge density at the IL cation, when compared to the C1 and C3 substitutions, leading thus to favorable anion–cation interactions.³²

The $[\text{cation}(\text{anion})_2]^-$ aggregates formed by ionic liquids containing the anions Cl^- , $[\text{BF}_4]^-$, $[\text{PF}_6]^-$, $[\text{CF}_3\text{SO}_3]^-$, and $[\text{N}(\text{CF}_3\text{SO}_2)_2]^-$ combined with the 1-butyl-3-methylimidazolium cation were also investigated using the same methodology. The relative interaction energies (as well as the computational dissociation energies that will be discussed below) versus the anionic radius³³ is depicted in Figure 6. The linear dependence observed in Figure 6 reveals that the interaction strength decreases with the increase of the anionic radius. This fact seems to be related to a decrease on the anion charge densities with the ionic radius increase, which is directly reflected on the cation–anion cohesion energy.

Quantum Chemical Calculations. To obtain further insights into the cation–anion interactions taking place in ionic liquids, as well as to gather a comprehensive study on the influence of the ILs' structural characteristics through their dissociation energies, quantum chemical calculation for the ion pairs $[(\text{cation})_2\text{-anion}]^+$ and $[(\text{anion})_2\text{cation}]^-$ were carried out. The $[\text{C}_4\text{mim}]$ -based ILs with the anions Cl^- , $[\text{BF}_4]^-$, $[\text{PF}_6]^-$, $[\text{TfO}]^-$, and

$[\text{NTf}_2]^-$, as well as $[\text{C}_4\text{C}_1\text{mim}][\text{NTf}_2]$, were investigated at the B3LYP/6-31+G(d) level of theory. The dissociation energies were estimated on the basis of the BSSE corrected electronic energies while considering the reactions presented in Scheme 1.

Scheme 1. Reactions Considered on the Dissociation Energies Estimation for the Studied Species



For each optimized structure, no imaginary harmonic vibrational frequencies were encountered, suggesting that an energetic minimum was obtained in all cases. The electronic energies (E_{ele}) and the BSSE corrected electronic energies [$E_{\text{ele(BSSE)}}$] for each species are presented in the Supporting Information (Table S2).

Table 3 reports the dissociation energies estimated, on the basis of the BSSE corrected electronic energies, for the ionic liquids studied. The BSSE uncorrected and corrected dissociation energies, in kilojoules per mole, are presented in the Supporting Information (Table S2). The difference between BSSE corrected and uncorrected values for the derived dissociation energies is small due to the BSSE energy correction compensation. Nevertheless, it was considered in this work.

Table 3. Calculated Dissociation Energies, Based on the BSSE Corrected Electronic Energies, $E_{\text{ele(BSSE)}}$, for the Considered ILs

| precursors | $E_{\text{diss(BSSE)}}^a/\text{eV}$ | | |
|--|---|---|--------------------------------------|
| | $[(\text{cation})\text{-}(\text{anion})]$ | $[\text{cation}\text{-}(\text{anion})_2]^-$ | $[(\text{cation})_2\text{-anion}]^+$ |
| $[\text{C}_4\text{mim}]\text{Cl}$ | 3.85 | 1.31 | 1.42 |
| $[\text{C}_4\text{mim}][\text{BF}_4]$ | 3.53 | 1.14 | 1.27 |
| $[\text{C}_4\text{mim}][\text{PF}_6]$ | 3.28 | 1.06 | 1.16 |
| $[\text{C}_4\text{mim}][\text{TfO}]$ | 3.42 | 1.12 | 1.20 |
| $[\text{C}_4\text{mim}][\text{NTf}_2]$ | 3.16 | 1.03 | 1.18 |
| $[\text{C}_4\text{C}_1\text{mim}][\text{NTf}_2]$ | 2.96 | 0.87 | 1.00 |

^a All the calculations were performed at the B3LYP/6-31+G(d) level of theory.

Corroborating the literature results,³⁴ two local minima geometries were found for the $[\text{C}_4\text{mim}][\text{NTf}_2]$ ionic pair, with a

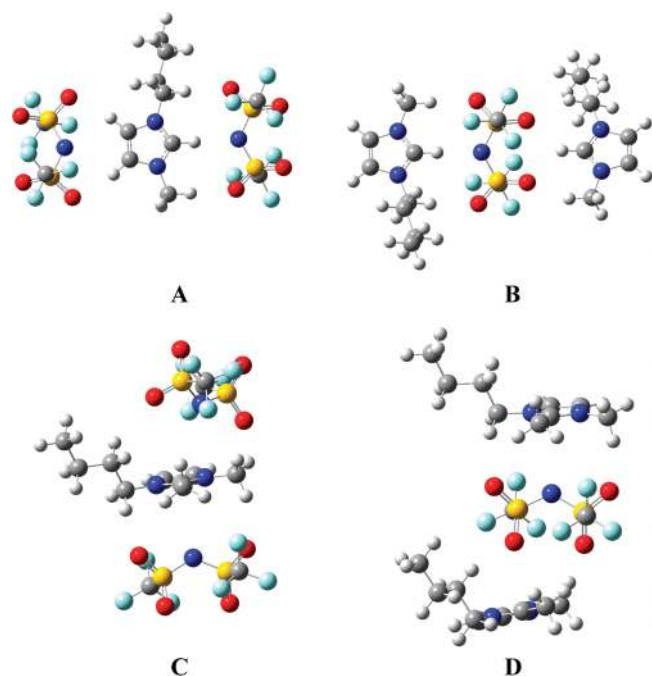


Figure 7. Schematic view of the optimized geometries (B3LYP/6-31+G(d)) of the IL aggregates, for $[\text{C}_4\text{mim}][\text{NTf}_2]$ and $[\text{C}_4\text{C}_1\text{mim}][\text{NTf}_2]$: (A) $[\text{C}_4\text{mim}][(\text{NTf}_2)_2]^-$; (B) $[(\text{C}_4\text{mim})_2][\text{NTf}_2]^+$; (C) $[\text{C}_4\text{C}_1\text{mim}][(\text{NTf}_2)_2]^-$; (D) $[(\text{C}_4\text{C}_1\text{mim})_2][\text{NTf}_2]^+$.

small energetic differentiation ($2.9 \text{ kJ} \cdot \text{mol}^{-1}$). Related information is presented in the Supporting Information (Figure S1). The difference between the two geometries is related to the $[\text{C}_4\text{mim}]^+$ position around $[\text{NTf}_2]^-$. The schematic views of the optimized geometries of the $[(\text{cation})_2\text{anion}]^+$ and $[(\text{anion})_2\text{cation}]^-$ aggregates for $[\text{C}_4\text{mim}][\text{NTf}_2]$ are depicted in Figure 7. The most stable geometries found in both cases are those that consider the ions aligned in the plane direction of the imidazolium ring. For $[\text{C}_4\text{C}_1\text{mim}][\text{NTf}_2]$ -related aggregates (Figure 7), the most stable geometries were found with the ions aligned perpendicularly to the plane of the ring, due to the hydrogen substitution at C2 by a bulk methyl group.

Energy experimental results, $E_{\text{cm},1/2}$, and the quantum chemical results, $E_{\text{diss(BSSE)}}$, as a function of the anionic radius³³ in the $[\text{cation}(\text{anion})_2]^-$ aggregates of the $[\text{C}_4\text{mim}]$ -based ILs with anions Cl^- , $[\text{BF}_4]^-$, $[\text{PF}_6]^-$, $[\text{TfO}]^-$, and $[\text{NTf}_2]^-$, are presented in Figure 6. As previously observed for $E_{\text{cm},1/2}$, the obtained quantum chemical estimations of the dissociation energy, $E_{\text{diss(BSSE)}}$, also show a good linear dependence of the anionic radius. This pattern reflects the decrease of the electrostatic cation–anion attraction potential. A good correlation among the results obtained by computational chemistry, at the B3LYP/6-31+G(d) level of theory, and the experimental results was found (1.0 ± 0.2 slope coefficient), with an energetic offset of -0.52 eV , which is related to the different energetic referential scale adopted for $E_{\text{cm},1/2}$. The comparison between the experimental $E_{\text{cm},1/2}$ values with the BSSE corrected dissociation energies obtained by quantum chemical calculations, $E_{\text{diss(BSSE)}}$, is presented in the Supporting Information (Figure S2).

Besides the effect of the ionic liquid anion on the dissociation energies, the effect of the most acidic hydrogen substitution at C2 in the imidazolium ring by a methyl group was also evaluated by quantum chemical calculations for the ion pairs $[\text{C}_4\text{mim}][\text{NTf}_2]$

and $[\text{C}_4\text{C}_1\text{mim}][\text{NTf}_2]$ and the corresponding aggregates $[(\text{cation})_2\text{NTf}_2]^+$ and $[(\text{NTf}_2)_2\text{cation}]^-$. An energetic difference of $20 \text{ kJ} \cdot \text{mol}^{-1}$ for the calculated ion pairs dissociation energy between $[\text{C}_4\text{mim}][\text{NTf}_2]$ and $[\text{C}_4\text{C}_1\text{mim}][\text{NTf}_2]$ was previously reported.³⁵ For the $[(\text{cation})_2\text{NTf}_2]^+$ and $[(\text{NTf}_2)_2\text{cation}]^-$ aggregates, the same magnitude of energetic difference ($15 \text{ kJ} \cdot \text{mol}^{-1}$) for the ions separation was obtained. This difference could be partially attributed to the hydrogen bonding between the hydrogen present at C2 and the bis[(trifluoromethyl)sulfonyl]imide anion in $[\text{C}_4\text{mim}][\text{NTf}_2]$. The higher dissociation energy for the separation of the cation in the $[(\text{C}_4\text{mim})_2\text{NTf}_2]^+$ aggregate compared with the $[(\text{C}_4\text{C}_1\text{mim})_2\text{NTf}_2]^+$ was also observed experimentally in this work, with values of relative interaction energies of 0.491 and 0.426 eV , respectively. Other experimental results, and also supported by quantum chemical calculations, show that the dissociation energy for the cation separation in $[(\text{C}_4\text{mim})_2\text{anion}]^+$ is significantly higher ($15 \text{ kJ} \cdot \text{mol}^{-1}$) than the anion separation in the $[\text{C}_4\text{mim}(\text{anion})_2]^-$ aggregate. The higher dissociation energy, inherent to the cation separation, in $[(\text{C}_4\text{mim})_2\text{anion}]^+$ is again related to the additional hydrogen at C2 in the imidazolium cation.

Evaluation of the Relative Cation–Anion Interaction Strengths versus Ionic Liquids Surface Tensions. Besides the studies on the physicochemical properties of ionic liquids and their dependence on the alkyl chain length, cation family and anionic species,^{6–8} a study regarding the relationship between interaction energies of IL ion pairs, obtained by ab initio calculations, and the ionic conductivity, was reported by Watanabe et al.⁹ The authors⁹ concluded that the electrostatic interaction is mainly responsible for the ionic attraction, with a nonnegligible contribution from induction effects. It was also shown⁹ that the magnitude and directionality of the interaction energy play a crucial role in determining the ionic dissociation/association dynamics in the ionic liquid. Nevertheless, a close relationship between the values of the calculated interaction energies and the experimental properties, such as melting point, density, self-diffusion coefficients, and molar conductivities, could not be found.⁹ In the same line of research, and due to the availability of surface tensions of several ionic liquids studied in this work,^{36–38} the correlation between the magnitude of such property and the relative interaction energies obtained by the mass spectrometry experiments was investigated.

In Figure 8 the surface tensions (σ) and $E_{\text{cm},1/2}$ are represented as a function of the alkyl chain length for $[\text{C}_n\text{mim}][\text{NTf}_2]$ ILs with $n = 1–10$, and as a function of anion size in 1-butyl-3-methylimidazolium-based ionic liquids. The surface tensions present a pattern similar to that of the relative interaction energies as a function of the IL structural features. An initial decrease in the magnitude of both properties toward a constant value, achieved for $n > 5$ is observed. Surface tensions also display a nearly linear decrease with the increase of the size of the IL anion, in a trend that emulates the relative interaction energies.

The relative orientation of the cations and the anions at the surface has been postulated as determinant for the ionic liquids surface tension. For butyl-imidazolium-based ILs, two orientation models have been proposed for the surface layer:³⁹ one where the butyl chains are parallel to the surface and the other where the chains are normal to the surface. It has also been shown that the relative location of cation and anion depends on the ionic composition of the ionic liquid which could be related to the competition between Coulombic/polar interactions at the ring and the alkyl chain–chain interactions.⁴⁰ Thus, it seems

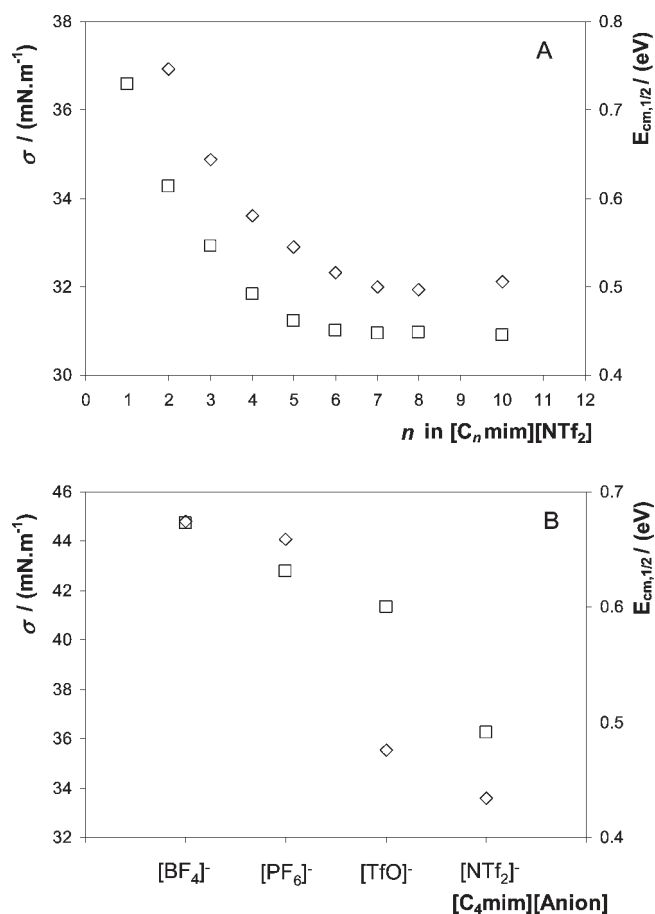


Figure 8. Dependence of the surface tension (σ) of pure ILs at 293.15 K (\diamond),^{36,37} and relative energies of dissociation of the $[(\text{cation})_2(\text{anion})]^+$ aggregates (\square), with the cation side alkyl chain length for the $[C_n\text{mim}][\text{NTf}_2]$ series (A) and with the anion nature in $[C_4\text{mim}][\text{Anion}]$ -based ILs (B).

reasonable to assume that surface orientation is dependent on the relative cation–anion interaction energies which would explain the close relationship observed between the surface tension and the experimental mass spectrometry data obtained for the relative ionic energies. However, additional care has to be taken in order to not oversimplify the interpretation of the results. For instance, the introduction of a methyl substituent in the position C2 of the imidazolium ring of $[C_4\text{mim}][\text{NTf}_2]$, leading to $[C_4C_1\text{mim}][\text{NTf}_2]$, decreases considerably the interaction energy while the opposite behavior was found for the surface tension.³⁸ This is probably related with a greater ordering of the IL at the air–liquid interface which is not reflected at the bulk.

CONCLUSIONS

A systematic study on the relative anion–cation interaction energies of imidazolium-, pyridinium-, pyrrolidinium-, and piperidinium-based ionic liquids was carried out in this work by electrospray tandem mass spectrometry (ESI-MS-MS). The results on the cation–anion relative interactions were interpreted in terms of the influence of anion size, cation core, charge dispersion, and steric hindrance. It was shown that the effect of the anion and the replacement of the most acidic hydrogen at C2

at the imidazolium ring by a methyl group are in particular agreement with the dissociation energies assessed by quantum chemical calculations. For all of the studied anions, a higher dissociation energy derived from the cation separation in the $[(C_4\text{mim})_2\text{anion}]^+$ aggregates than that derived from the anion separation from $[C_4\text{mim}(\text{anion})_2]^-$ is observed. The impact of the ion interaction strengths here measured in common ionic liquid thermophysical properties was illustrated using surface tension data. It was shown that this property follows a trend analogous to the relative interaction energies determined by mass spectrometry regarding both the cation alkyl chain length and the anion size.

ASSOCIATED CONTENT

S Supporting Information. Tables listing electronic energies and BSSE dissociation energies, and figures showing schematic view of local minima geometries and electronic energies and dissociation energies vs relative interaction energies. This material is available free of charge via the Internet at <http://pubs.acs.org>.

AUTHOR INFORMATION

Corresponding Author

*Tel.: +351-234-370200. Fax: +351-234-370084. E-mail: afernandes@ua.pt.

ACKNOWLEDGMENT

Thanks are due to Fundação para a Ciência e a Tecnologia (FCT), Lisbon, Portugal, for the project PTDC/QUI/72903/2006 and to FEDER for financial support to Centro de Investigação em Química, University of Porto, Portugal. M.A.A.R. and M.G.F. also thank FCT and the European Social Fund (ESF) under the third Community Support Framework (CSF) for the award of research grants with references SFRH/BD/60513/2009 and SFRH/BPD/41781/2007, respectively.

REFERENCES

- (1) Plechkova, N. V.; Seddon, K. R. *Chem. Soc. Rev.* **2008**, *37*, 123.
- (2) Smiglak, M.; Metlen, A.; Rogers, R. D. *Acc. Chem. Res.* **2007**, *40*, 1182.
- (3) Hough, W. L.; Smiglak, M.; Rodriguez, H.; Swatloski, R. P.; Spear, S. K.; Daly, D. T.; Pernak, J.; Grisel, J. E.; Carliss, R. D.; Soutullo, M. D.; Davis, J. H.; Rogers, R. D. *New J. Chem.* **2007**, *31*, 1429.
- (4) Izgorodina, E. I.; Bernard, U. L.; MacFarlane, D. R. *J. Phys. Chem. B* **2009**, *113*, 7064.
- (5) Tokuda, H.; Hayamizu, K.; Ishii, K.; Susan, M. A. B. H.; Watanabe, M. *J. Phys. Chem. B* **2004**, *108*, 16593.
- (6) Tokuda, H.; Hayamizu, K.; Ishii, K.; Susan, M. A. B. H.; Watanabe, M. *J. Phys. Chem. B* **2005**, *109*, 6103.
- (7) Tokuda, H.; Ishii, K.; Susan, M. A. B. H.; Tsuzuki, S.; Hayamizu, K.; Watanabe, M. *J. Phys. Chem. B* **2006**, *110*, 2833.
- (8) Jin, H.; O'Hare, B.; Dong, J.; Arzhantsev, S.; Baker, G. A.; Wishart, J. F.; Benese, A. J.; Maroncelli, M. *J. Phys. Chem. B* **2008**, *112*, 81.
- (9) Tsuzuki, S.; Tokuda, H.; Hayamizu, K.; Watanabe, M. *J. Phys. Chem. B* **2005**, *109*, 16474.
- (10) Borodin, O. *J. Phys. Chem. B* **2009**, *113*, 12353.
- (11) Bandrés, I.; Giner, B.; Artigas, H.; Royo, F. M.; Lafuente, C. *J. Phys. Chem. B* **2008**, *112*, 3077.
- (12) Logotheti, G.; Ramos, J.; Economou, I. G. *J. Phys. Chem. B* **2009**, *113*, 7211.

- (13) Osada, R.; Hoshino, T.; Okada, K.; Ohmasa, Y.; Yao, M. *J. Chem. Phys.* **2009**, *130*, 184705.
- (14) López-Martin, I.; Burello, E.; Davey, P. N.; Seddon, K. R.; Rothenberg, G. *ChemPhysChem* **2007**, *8*, 690.
- (15) Hart, K. J.; McLuckey, S. A. *J. Am. Soc. Mass Spectrom.* **1994**, *5*, 250.
- (16) Colorado, A.; Brodbelt, J. S. *J. Am. Soc. Mass Spectrom.* **1996**, *7*, 1116.
- (17) Zhang, J.; Brodbelt, J. S.; Wang, J. *J. Am. Soc. Mass Spectrom.* **2005**, *16*, 139.
- (18) Satterfield, M.; Brodbelt, J. S. *Inorg. Chem.* **2001**, *40*, 5393.
- (19) Jellen, E. E.; Chappell, A. M.; Ryzhov, V. *Rapid Commun. Mass Spectrom.* **2002**, *16*, 1799.
- (20) Vinokur, N.; Ryzhov, V. *J. Mass Spectrom.* **2004**, *39*, 1268.
- (21) Hayes, L. A.; Chappell, A. M.; Jellen, E. E.; Ryzhov, V. *Int. J. Mass Spectrom.* **2003**, *227*, 111.
- (22) Mazzitelli, C. L.; Wang, J.; Smith, S. I.; Brodbelt, J. S. *J. Am. Soc. Mass Spectrom.* **2007**, *18*, 1760.
- (23) Forbes, M. W.; Volmer, D. A.; Francis, G. J.; Böhme, D. K. *J. Am. Soc. Mass Spectrom.* **2005**, *16*, 779.
- (24) Fernandes, A. M.; Coutinho, J. A. P.; Marrucho, I. M. *J. Mass Spectrom.* **2009**, *44*, 144.
- (25) David, W. M.; Brodbelt, J. S. *J. Am. Soc. Mass Spectrom.* **2003**, *14*, 383.
- (26) Becke, A. D. *J. Chem. Phys.* **1993**, *98*, 5648.
- (27) Becke, A. D. *Phys. Rev. A* **1988**, *38*, 3098.
- (28) Boys, S.; Bernardi, F. *Mol. Phys.* **1970**, *19*, 553.
- (29) Frisch, M. J.; Trucks, G. W.; Schlegel, H. B.; Scuseria, G. E.; Robb, M. A.; Cheeseman, J. R.; Montgomery, J. A., Jr.; Vreven, T.; Kudin, K. N.; Burant, J. C.; Millam, J. M.; Iyengar, S. S.; Tomasi, J.; Barone, V.; Mennucci, B.; Cossi, M.; Scalmani, G.; Rega, N.; Petersson, G. A.; Nakatsuji, H.; Hada, M.; Ehara, M.; Toyota, K.; Fukuda, R.; Hasegawa, J.; Ishida, M.; Nakajima, T.; Honda, Y.; Kitao, O.; Nakai, H.; Klene, M.; Li, X.; Knox, J. E.; Hratchian, H. P.; Cross, J. B.; Bakken, V.; Adamo, C.; Jaramillo, J.; Gomperts, R.; Stratmann, R. E.; Yazyev, O.; Austin, A. J.; Cammi, R.; Pomelli, C.; Ochterski, J. W.; Ayala, P. Y.; Morokuma, K.; Voth, G. A.; Salvador, P.; Dannenberg, J. J.; Zakrzewski, V. G.; Dapprich, S.; Daniels, A. D.; Strain, M. C.; Farkas, O.; Malick, D. K.; Rabuck, A. D.; Raghavachari, K.; Foresman, J. B.; Ortiz, J. V.; Cui, Q.; Baboul, A. G.; Clifford, S.; Cioslowski, J.; Stefanov, B. B.; Liu, G.; Liashenko, A.; Piskorz, P.; Komaromi, I.; Martin, R. L.; Fox, D. J.; Keith, T.; Al-Laham, M. A.; Peng, C. Y.; Nanayakkara, A.; Challacombe, M.; Gill, P. M. W.; Johnson, B.; Chen, W.; Wong, M. W.; Gonzalez, C.; Pople, J. A. *Gaussian 03*, Revision C.02; Gaussian: Pittsburgh, PA, 2004.
- (30) Sleno, L.; Volmer, D. J. *Mass Spectrom.* **2004**, *39*, 1091.
- (31) Izgorodina, E. I.; Forsyth, M.; MacFarlane, D. R. *Aust. J. Chem.* **2007**, *60*, 15.
- (32) Freire, M. G.; Neves, C. M. S. S.; Shimizu, K.; Bernardes, C.; Marrucho, I. M.; Coutinho, J. A. P.; Canongia Lopes, J. N.; Rebelo, L. P. N. *J. Phys. Chem. B* **2010**, *114*, 15925.
- (33) Zhang, S.; Sun, N.; He, X.; Lu, X.; Zhang, X. *J. Phys. Chem. Ref. Data* **2006**, *35*, 1475.
- (34) Chiu, Y.-H.; Gaeta, G.; Levandier, D. J.; Dressler, R. A.; Boatz, J. A. *Int. J. Mass Spectrom.* **2007**, *265*, 146.
- (35) Kirchner, B. *Top. Curr. Chem.* **2010**, *290*, 213.
- (36) Freire, M. G.; Carvalho, P. J.; Fernandes, A. M.; Marrucho, I. M.; Queimada, A. J.; Coutinho, J. A. P. *J. Colloid Interface Sci.* **2007**, *314*, 621.
- (37) Carvalho, P. J.; Freire, M. G.; Marrucho, I. M.; Queimada, A. J.; Coutinho, J. A. P. *J. Chem. Eng. Data* **2008**, *53*, 1346.
- (38) Carvalho, P. J.; Neves, C. M. S. S.; Coutinho, J. A. P. *J. Chem. Eng. Data* **2010**, *55*, 3807.
- (39) Sloutskin, E.; Ocko, B. M.; Tamam, L.; Kuzmenko, I.; Gog, T.; Deutsch, M. *J. Am. Chem. Soc.* **2005**, *127*, 7796.
- (40) Santos, C. S.; Baldelli, S. *J. Phys. Chem. B* **2009**, *113*, 923.